

Eco-Friendly Synthesis of Seed Extract-Mediated ZnO Nanoparticles for Photocatalytic Degradation of Methylene Blue Dye

Minbale Gashu ^{1,*}, Getahun Yigezu ¹, Neway Belachew ¹, Jemal M. Yassin ¹, Asfaw Negash ^{1,*}

¹ Department of Chemistry, Debre Berhan University, Debre Berhan, P.O. BOX 445, Ethiopia; minbalegashu@dbu.edu.et (M.G.); getahunyigezu34@gmail.com (G.Y.); neway@dbu.edu.et (N.B.); jemalmohammed@dbu.edu.et (J.M.Y.); asfawnegash@dbu.edu.et (A.N.);

* Correspondence: minbalegashu@dbu.edu.et; asfawnegash@dbu.edu.et;

Received: 18.06.2024; Accepted: 2.01.2025; Published: 20.12.2025

Abstract: Organic pollutants found in industrial wastewater, such as dyes, are unsafe for people and aquatic life due to the extensive environmental and human health risks. Given the environmental benefits, *Abelmoschus esculentus* (okra) seed-mediated synthesis of zinc oxide (ZnO) nanoparticles (NPs) is used for the photocatalytic degradation of methylene blue (MB) as a model organic pollutant under direct sunlight. Physicochemical properties of seed-mediated ZnO NPs were determined by XRD, SEM-EDS, FTIR, and a UV-Vis spectrophotometer, which evidenced the successful synthesis of the as-obtained sample using an eco-friendly approach. The photocatalytic degradation efficiency of ZnO NPs to degrade MB was found to be 94.7% at optimized working conditions, such as pH (10), catalyst load (70 mg), initial MB concentration (10 mg L⁻¹), and contact time (90 min), while 46.0% under a dark system. This study demonstrates a pseudo-first-order kinetic model for the photocatalytic degradation of MB using eco-friendly, synthesized ZnO NPs as the photocatalyst. Therefore, the as-synthesized okra seed-mediated ZnO NP was a potential photocatalyst for the degradation of MB dye from aqueous solutions.

Keywords: eco-friendly; *Abelmoschus esculentus* seed; ZnO NPs; photocatalyst; MB.

© 2025 by the authors. This article is an open-access article distributed under the terms and conditions of the Creative Commons Attribution (CC BY) license (<https://creativecommons.org/licenses/by/4.0/>), which permits unrestricted use, distribution, and reproduction in any medium, provided the original work is properly cited. The authors retain copyright of their work, and no permission is required from the authors or the publisher to reuse or distribute this article, as long as proper attribution is given to the original source.

1. Introduction

15% of the world's total output of dye products is discharged into the environment as dye wastewater [1]. This considerable amount of ecologically unsafe dyes produced by industries such as textile, paper/pulp, plastic, leather, food, pharmaceutical, and cosmetics seriously pollutes groundwater resources [2-7]. Photosynthesis in such dye-polluted water systems is limited because the dye can block light penetration. Methylene blue (MB), the commonly used cationic industrial dye, is toxic to humankind, animals, and aquatic organisms [8-10].

In countries like Ethiopia, the production and use of dyes are increasing without proper treatment. The dyes harm the environment and aquatic life, and pose serious health threats (toxicity) to humans upon degradation [3,5-7,11,12]. Since MB is environmentally stable and challenging to remove in sewage treatment, its removal is mandatory to protect the environment and support life [8-10,13,14]. Given the potential toxicity of such dyes and their

environmental consequences, there is a significant need for researchers to develop eco-friendly methods to remove dyes from industrial effluents prior to their disposal, thereby minimizing their impact on human and aquatic environments. Photocatalytic degradation [6,7,15-22] is one of the most widely used methods for eliminating organic dye pollutants through mineralization, leaving no environmentally unwanted residues [3,9,10, 23].

Semiconductors are commonly used as photocatalysts because they generate highly reactive hydroxyl radicals and holes that degrade a wide variety of organic compounds through oxidation [3,24]. The current study focuses on exploiting semiconductor metal oxide nanomaterials, such as zinc oxide (ZnO), for environmental applications due to their unique optical, electronic, mechanical, magnetic, and chemical properties [3,14-22,24]. Zinc oxide nanoparticles (ZnO NPs) have been reported as suitable photocatalysts for the removal of organic dyes [24,25] due to their low toxicity, direct wide bandgap, and photo-corrosion stability [3,4,20-22].

Sol-gel processing, mechanical milling, organometallic synthesis, microwave, spray pyrolysis, thermal evaporation, and precipitation are commonly used chemical methods for synthesizing ZnO NPs [15,23,25]. However, these techniques repeatedly use highly reactive and environmentally harmful organic solvents and toxic reducing agents. Therefore, the use of plant-derived natural products for the eco-friendly synthesis of ZnO NPs is an alternative and timely approach [3,7,8,25].

A. esculentus, known as lady's finger or okra, is likely to originate in Ethiopia and spread all over the world. Okra pods supply food nutrients such as carbohydrates, minerals, and vitamins, whereas the seeds serve as alternative sources of protein, fat, fiber, and sugar. The plant is also rich in natural products, such as flavonoids, which can reduce the risk of hyperlipidemia, stroke, diabetes, cardiovascular diseases, obesity, and cancers due to their antioxidant properties. The whole plant is edible as it is a powerhouse of valuable nutrients [26-34].

Hydroxyl and carboxyl functional groups of compounds in plant extracts interact electrostatically with metal ions and act as capping agents to prevent the growth of ZnO crystals [3,8,24,35]. The photocatalytic potential of ZnO NPs was evaluated by the degradation of MB under direct sunlight irradiation. Data reported on *A. esculentus* seed extract-synthesized ZnO NPs for the degradation of MB by photocatalysis were not found in the literature. In this work, we reported an eco-friendly synthesis of ZnO NPs using aqueous seed extract of *A. esculentus* for the photocatalytic degradation of MB dye.

2. Materials and Methods

2.1. Materials.

Chemicals and reagents used for this work include: sodium hydroxide pellets (NaOH, 99.8%, Alphax Chemical), zinc acetate dihydrate ($\text{Zn}(\text{CH}_3\text{CO}_2)_2 \cdot 2\text{H}_2\text{O}$, 99.5%, Loba Chemie), and methylene blue ($\text{C}_{16}\text{H}_{18}\text{N}_3\text{SCl}$, 82%, Loba Chemie) without further purification. Double-distilled water was used throughout the whole experiment.

2.2. Preparation of aqueous extract and phytochemical screening test.

Seeds of *A. esculentus* were collected from Amhara Regional State (Ethiopia), North Showa Zone, Shewarobit town, village 02, at the beginning of January 2021, rinsed with tap water, then with double-distilled water, and dried in the shade for several weeks at room

temperature. The dried seeds were ground and packed in plastic bags until use. 20.0 g of the seed powder (20 %) of the plant was boiled in double-distilled water at 60°C for 30 min. The aqueous extract was then cooled, filtered through Whatman No. 1 filter paper, and stored at 4°C for further use. A phytochemical analysis of *A. esculentus* aqueous seed extract was performed following known protocols [36].

2.3. Seed-mediated synthesis of ZnO NPs.

A facile and eco-friendly precipitation method was used to form ZnO NPs in the presence of aqueous seed extract of *A. esculentus*. In particular, 0.5 g of $\text{Zn}(\text{CH}_3\text{COO})_2 \cdot 2\text{H}_2\text{O}$ (0.019 M) was added to about 100 mL of double-distilled water containing an aqueous seed extract (20 %), and the mixture was gently stirred in a conical flask (250 mL) under a reflux condenser at 60°C for 1 h. The solution pH was adjusted to pH 10 using 0.01 M NaOH. The resulting solution was centrifuged at 15,000 rpm for 10 min and washed with double-distilled water. The white-yellow paste was then dried in an oven at 100°C for 4 h to remove adsorbed water. The resultant solid sample was labelled as ZnO NPs. Different extract concentrations were used to investigate the role of the plant extract on the crystal structure of ZnO NPs at the test reaction conditions: constant pH (10), reaction time (1 h), precursor amount (50 mL, 0.019 M), and temperature (60°C) [3,15].

2.4. Characterization of ZnO NPs.

The structures of different seed-mediated ZnO NPs were characterized by X-ray diffraction (XRD) using SHIMADZU XRD-7000 equipped with an X-ray source of Cu $\text{K}\alpha$ radiation (wavelength of 1.54056 Å), operating voltage of 40.0 kV and 30 mA with 2θ range: 5.0-90°. The crystallite size was estimated from Debye-Scherrer's equation using the most intense peak of the as-synthesized samples. Fourier transform infrared (FTIR) spectra of aqueous extract of *A. esculentus* seed and seed extract-mediated ZnO NPs were recorded using a Perkin Elmer FTIR spectrometer in the range 400-4000 cm^{-1} in a KBr pellet method in order to identify the surface functional groups present in the extract and ZnO NPs [24,37]. The optical properties of the as-synthesized solid sample were determined by scanning over 200-800 nm using a UV-Vis absorption spectrophotometer (Model: Optizen POP; S.N.: 5U4604-122021-00, Korea); samples were dispersed in deionized water before analysis. Morphologies and composition or particle distribution of the as-synthesized photocatalyst were determined by scanning electron microscopy (SEM), hyphenated with an energy dispersive spectroscopy (EDS) detector and a backscattered detector instrument.

The crystal structure and phase purity of ZnO NPs were investigated using an X-ray diffractometer. The average crystallite size of the as-synthesized nanoparticles was determined from the XRD patterns using Scherrer's equation [3, 37, 38].

$$D = \frac{k\lambda}{\beta \cos \theta} \quad (1)$$

Where: D is crystallite size, k is Scherrer constant; λ is the X-ray source wavelength, which equals 0.15406 nm, β is the Full Width Half Maximum intensity (FWHM) in radians, and θ is the half diffraction (Bragg's) angle. The SurfCharJ 1q plugin in Image J software was used to investigate the surface roughness of ZnO NPs [39].

2.5. Point of zero charge.

The pH of the point zero charge (PZC) of ZnO NPs was determined using the salt addition method [3] to examine surface charge as a function of pH, in which sodium chloride solution (30 mL, 0.01 M) was placed in a 100 mL Erlenmeyer flask. The pH was then adjusted to initial pH values (2, 4, 6, 8, 10, and 12) by either NaOH or HCl (0.01 M). 0.025 g of seed-mediated ZnO NPs was added to 30 mL of the initial concentration for a contact time of 24 h on a rotary shaker. The final pH was measured, and the ΔpH was calculated by the formula, $\text{pH}_{\text{final}} - \text{pH}_{\text{initial}}$. The PZC is obtained from the plot of initial pH vs ΔpH [23,3,40,41].

2.6. Photocatalytic degradation of MB dye.

The photocatalytic activity of the seed-mediated ZnO photocatalyst was evaluated by adding 0.030 g of the photocatalyst to 30 mL of an initial MB concentration (10 mg L⁻¹) and shaking for 2h on a rotary shaker at room temperature under direct sunlight irradiation [3,14-23]. The absorption maxima of the MB solution were recorded using a UV-Vis spectrophotometer, scanned at $\lambda_{\text{max}} = 664$ nm. The photocatalytic degradation under optimized conditions was investigated as a function of solution pH, contact time, catalyst dose, and initial MB concentration. The degradation efficiency of the process with respect to each parameter was calculated using the known equation [3,23].

$$\text{Degradation}(\%) = \frac{C_o - C_t}{C_o} \times 100 = \frac{A_o - A_t}{A_o} \times 100 \quad (2)$$

Where: C_0 (mg L⁻¹) is the initial concentration of MB, C_t (mg L⁻¹) is the concentration of MB after photodegradation at time t, and A_0 and A_t are the initial and at time t absorbance of MB.

To evaluate the effect of contact time, the experiment was conducted at 0, 30, 60, 90, 120 min, and 0.07 g of ZnO NPs. The effect of catalyst dose on the degradation efficiency of MB by ZnO NPs was examined at doses of 30, 50, 70, 90, and 110 mg in 10 mg L⁻¹ of MB, with a contact time of 2 h. The effect of the initial concentration of the MB dye solution on its degradation was studied by varying the concentration to 2.5, 5, 10, 15, and 20 mg L⁻¹, while keeping the photocatalyst load (70 mg) and contact time (2 h) constant.

2.7. Degradation kinetics.

In order to investigate the plausible photocatalytic degradation mechanism of ZnO NPs synthesized by aqueous seed extract of *A. esculentus*, a pseudo-first-order degradation kinetics model was employed.

3. Results and Discussion

3.1. Phytochemical analysis.

Phytochemical analysis of *A.esculentus* seed extract indicated the presence of metabolites such as flavonoids, phenols, and tannins that can act as capping agents during ZnO NPs synthesis (Table 1). The phytochemicals in the seed extract can also reduce the Zn²⁺ by donating electrons and stabilize the synthesized nanoparticles. For instance, phenolic compounds are important plant constituents that act as reducing agents [3].

Table 1. Qualitative phytochemical analysis of okra seed aqueous extract.

Chemical component	Chemical test	Color observed	Water extract
Tannin	Ferric chloride test	Dark green	+
Steroids	Salkowski test	Brownish-yellow	+
Flavonoids	Ferric chloride test	Yellow	++
Saponins	Wagner's test	Emulsion forms	+
Alkaloids	Ferric chloride test	Yellow(orange)	+
Phenols	Ferric chloride test	Brown precipitate	+

+ Presence

3.2. Synthesis of ZnO nanoparticles and their formation mechanism.

ZnO NPs were synthesized involving *A. esculentus* aqueous seed extract using zinc acetate dihydrate as a precursor. Its formation was confirmed by the appearance of a light yellow color due to the reaction of phenolic compounds, such as flavonoids in the extract, with zinc acetate dihydrate, following the reported reaction mechanism [3].

3.3. X-Ray Diffraction (XRD) analysis.

Figure 1 shows the XRD pattern of the as-synthesized ZnO via the precipitation method. Analysis of the XRD pattern of the NPs at different concentrations of plant extract revealed the formation of sharp peaks, free of impurities. The characteristic peaks of ZnO NPs appeared in the XRD, and all other peaks match well with standard data at JCPDS No. 00-036-1451 [41] for the hexagonal wurtzite crystal structure.

Table 2. Geometric parameters of ZnO NPs synthesized in different extract concentrations.

1% (a)				2% (b)				3% (c)			
2θ	d-spacing (Å)	FWHM (deg)	D (nm)	2θ	d-spacing (Å)	FWHM (deg)	D (nm)	2θ	d-spacing (Å)	FWHM (deg)	D (nm)
36.27	2.48	0.58	16.9	36.27	2.47	0.49	15.8	36.24	2.48	0.52	14.6
34.43	2.60	0.42	16.5	34.43	2.60	0.36	15.1	34.40	2.60	0.37	14.8
31.77	2.81	0.59	15.8	31.77	2.62	0.49	14.8	31.75	2.82	0.52	14.2
Average crystallite size			16.4				15.2				14.5

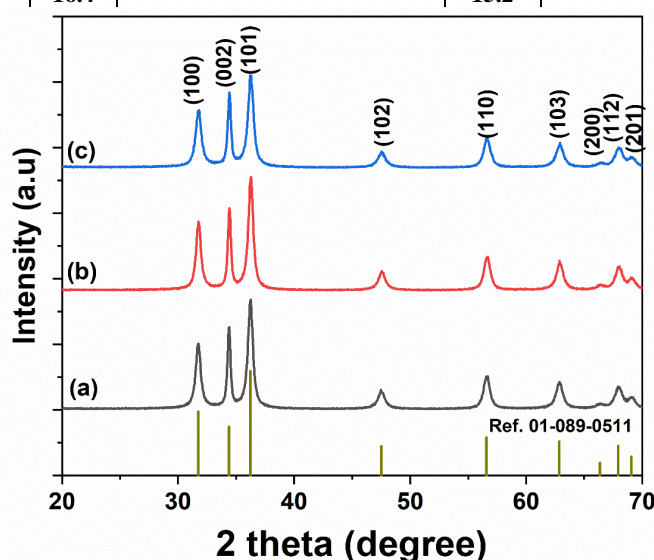


Figure 1. XRD patterns of ZnO reference and ZnO NPs synthesized with (a) 1% (black); (b) 2% (red); (c) 3% (blue) okra seed aqueous extracts.

Based on the diffraction peaks of ZnO NPs synthesized using 1% (a), 2% (b) and 3% (c) plant extracts (Figure 1, Table 2) the average crystallite size was calculated as 16.4 nm, 15.2 nm and 14.5 nm, respectively, and the data shows the participation of the chemical component of the plant material in the synthesis as capping and/or stabilizing agent. In the

course of crystallite size from 16.4 nm to 14.5 nm, a limitation of crystal growth is observed at higher concentrations of the plant extract than at lower ones in order to get small-sized NPs. The XRD patterns of the synthesized NPs demonstrate the formation of well-crystalline ZnO NPs, and the average crystallite size of the synthesized ZnO NPs was better than the previous report [3].

3.4. Scanning electron microscopy (FE-SEM) and energy dispersive X-ray spectroscopy (EDS).

As shown in Figure 2, the surface morphology and elemental composition of the as-synthesized ZnO NPs were investigated by the FE-SEM-EDX analysis. The FE-SEM images at different scales show the formation of aggregated ZnO NPs with surface porosity (Figure 2a-c). The 3D surface plot (Figure 2d) and the roughness intensity profile (Figure 2e) extracted from Figure 2c showed the high surface porosity of ZnO. The brighter (reddish) and darker (bluish) colors in Figure 2d showed the higher and lower grey values of the FE-SEM, respectively. The average surface roughness (Ra) of ZnO NPs is 41.18. EDS spectra (Figure 2f) show the presence of zinc and oxygen atoms, which evidence the successful synthesis of ZnO.

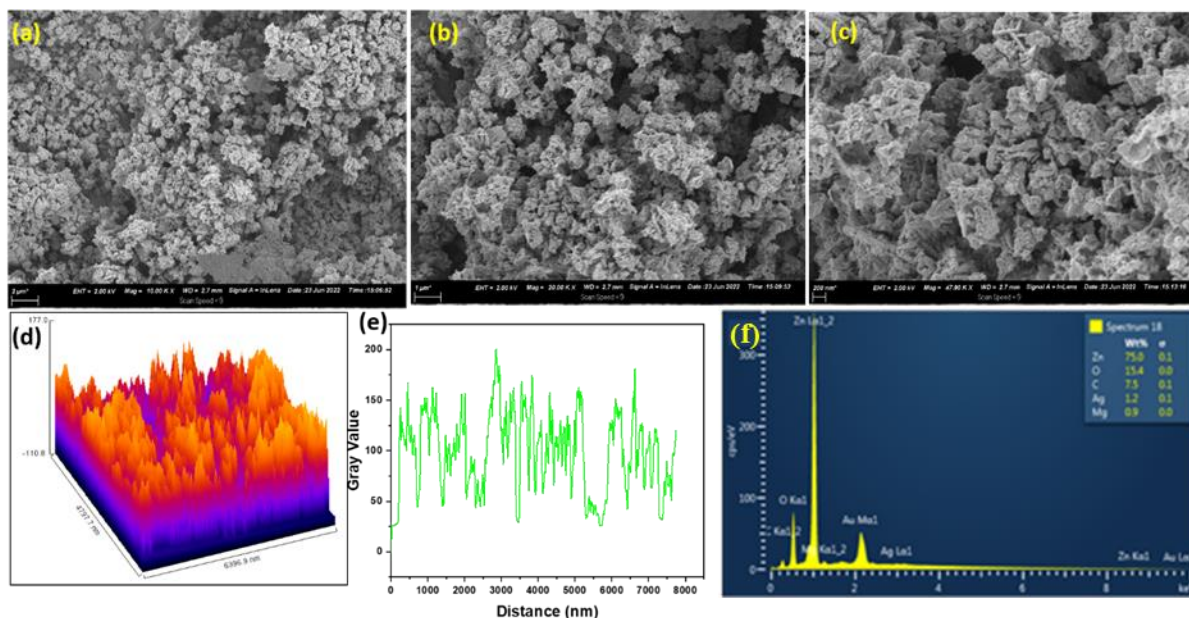


Figure 2. FE-SEM images of as-synthesized (a-c) ZnO NPs; (d) 3D surface plot; (e) roughness intensity profile; (f) EDS analysis result of ZnO sample.

3.5. UV-vis spectroscopy analysis.

The optical property of seed-mediated ZnO NPs was examined by UV-Vis absorption spectroscopy. The optical bandgap (E_g) of the ZnO NPs was calculated using the formula $E_g = \frac{1240}{\lambda_{edge}}$ (eV) from the absorption onset wavelength (λ_{edge}), which was 2.55 eV centered at 485 nm (Figure 3) [42]. The optical bandgap of the seed-mediated synthesized ZnO was narrowed to a bandgap (2.55 eV) compared to ZnO NPs synthesized via a sol-gel method, 3.10 eV [43]. This reduction in the optical bandgap, due to a decrease in particle size, is attributed to nanoscale electronic confinement, the so-called quantum confinement or quantum size effect. This, in turn, established the transition to lower energies and its low-dimensional quantum-size effect due to electron and hole confinement in the semiconductor matrix.

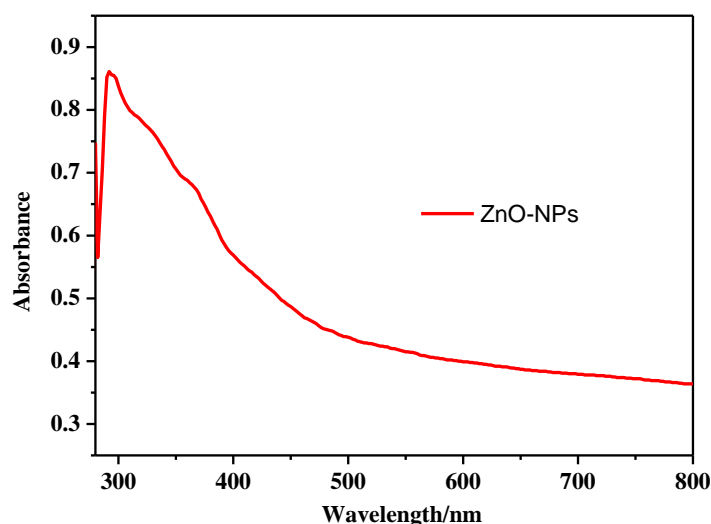


Figure 3. UV-vis spectra of ZnO NPs (1-44F, 3%).

3.6. Fourier transform infrared spectroscopy (FTIR) analysis.

Identification of the functional groups present in the aqueous okra seed extract and the synthesized nanomaterial using FTIR analysis was done, and it showed the presence of mainly –OH (3450 cm^{-1}) of phenolic and -OH ($1640, 745\text{ cm}^{-1}$) of absorbed water (Figure 4) in the former. The FTIR spectra of ZnO NPs prepared using the okra seed extracts of 1% (a), 2% (b), and 3% (c) (Figure 4) described a slight shift of absorption bands from that of the extract alone. The vibration band shifted from 3450 to 3390 cm^{-1} , which was due to O-H stretching. The FTIR characteristic peaks of the vibration observed at 555 cm^{-1} were due to the presence of Zn-O stretching vibration, which is in good agreement with the literature [37]. The newly observed vibration bands at 1590 cm^{-1} (C-C stretching), 1035 cm^{-1} (C-O), and 910 cm^{-1} (O-H) indicated the interactions among the natural products and zinc acetate to form ZnO NPs (Figure 4).

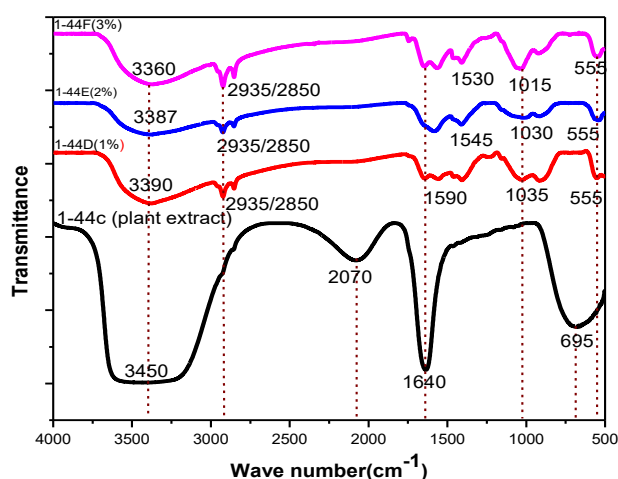


Figure 4. FTIR spectra of *A. esculentus* seeds extract (1-44C, black line) and seed-mediated ZnO NPs (1-44D, 1%, red), (1-44E, 2%, blue), and (1-44F, 3%, magenta).

3.7. Photocatalytic degradation study of MB dye.

3.7.1. Point of zero charge.

PZC is a pH-shift method used to determine the sign of the surface charge of metal oxide nanoparticles in terms of ΔpH [41,44]. The PZC for ZnO NPs was found to be 7.4 (Figure

5), and at pH less than 7.4, the photocatalytic surface becomes positive and attracts anions from the solution. As the pH of the solution is greater than 7.4, the catalyst surface becomes negative and attracts cations from the solution. Therefore, under such basic media, the cationic MB dye from aqueous solution can strongly interact electrostatically with the anionic surface of ZnO NPs photocatalyst. Subsequently, high photocatalytic degradation of MB dye was expected and observed [3,45].

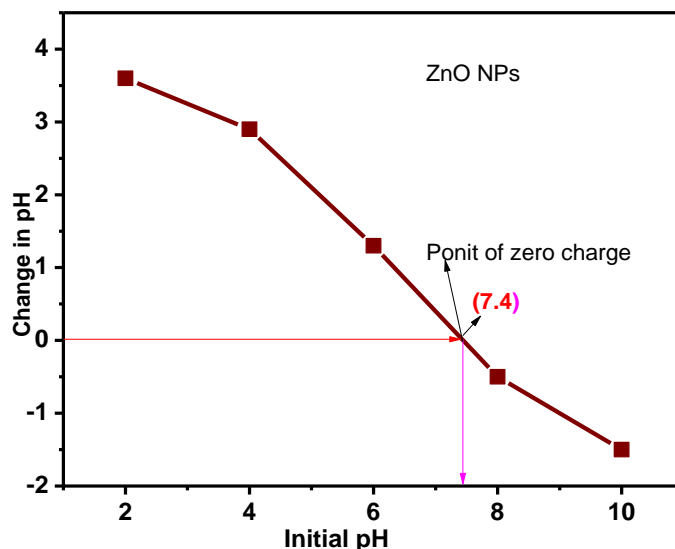


Figure 5. The pH at the point of zero charge for the ZnO sample.

3.7.2. Effect of pH.

Figure 6 shows the effect of solution pH on the degradation efficiency of ZnO NPs. The effect of pH on the degradation of MB dye with ZnO was investigated over a pH range of 2.0-12. The experiment showed high degradation efficiency of ZnO NPs at pH 10 within 2 h of irradiation, indicating that, as the pH is above the PZC, more negatively charged surfaces of the NPs were available for greater degradation of the MB dye.

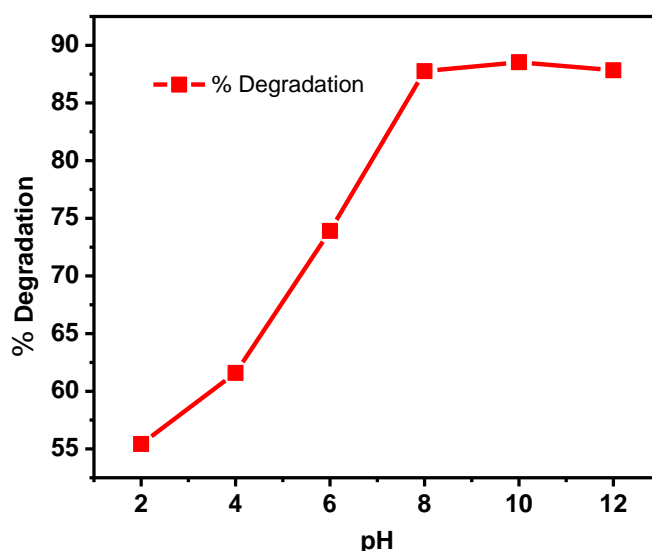


Figure 6. The effect of pH on the degradation of MB dye using ZnO NPs.

3.7.3. Effect of sunlight radiation.

The photocatalytic degradation potential was evaluated by monitoring the degradation of MB dye (30 mL of 10 mg L⁻¹) using ZnO NPs, with and without sunlight, over time. In this

study, a considerable amount of MB dye (94.7%) was degraded in the presence of sunlight radiation, compared to the dark (46.0%) (Figure 7).

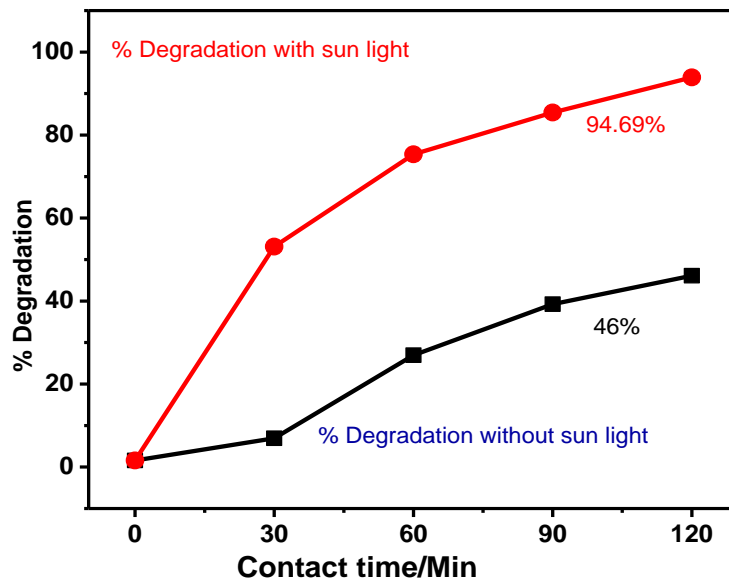


Figure 7. Degradation of MB in direct sunlight and in the dark as a function of time at pH 10.

3.7.4. Effect of ZnO photocatalyst dose.

The effect of the amount of ZnO photocatalyst on the degradation of the MB dye was investigated. The effect of ZnO NP dosage (30, 50, 70, 90, and 110 mg) on 30 mL of 10 mg L⁻¹ MB dye at pH 10 was studied. The results showed that increasing the nanoparticle dose improved degradation efficiency at 90 min, likely due to increased availability of active sites, as shown in Figure 8. Therefore, 70 mg of ZnO NPs was selected as the optimal photocatalyst dose for the degradation of 10 mg L⁻¹ of MB dye.

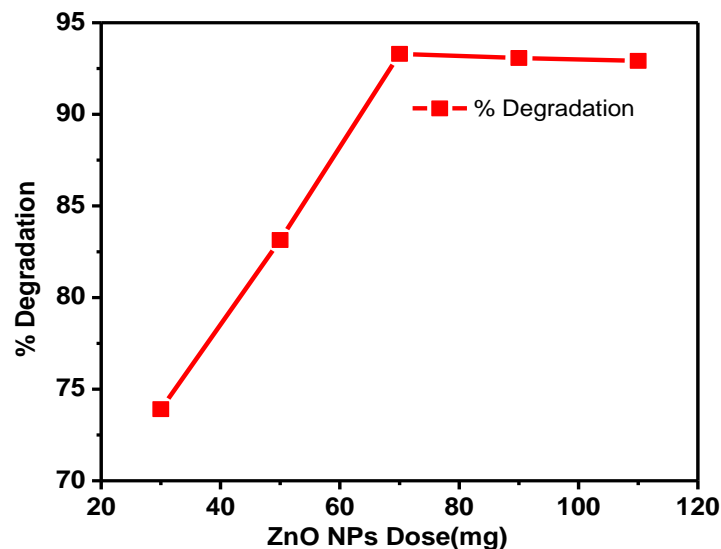


Figure 8. Effect of ZnO NPs dose on degradation of MB dye.

3.7.5. Effect of initial concentration of MB dye.

The effect of the initial concentration of the MB dye solution on the catalyst's degradation efficiency was studied by varying the initial concentration from 2.5, 5, 10, 15, and 20 mg L⁻¹ at an experimentally determined catalyst dose of 70 mg at pH 10 for 2 h. As shown in Figure 9, the catalyst's degradation efficiency decreased from 98.9% to 69.6% as the initial

MB concentration increased from 2.5 to 20 mg L⁻¹. This is because the number of active sites in the prepared nanoparticle is limited compared to the excess MB dye molecules, which prevents sunlight from reaching the catalyst surface. Hence, the production of hydroxyl radicals could be limited, resulting in decreased degradation efficiency of ZnO NPs toward the MB dye.

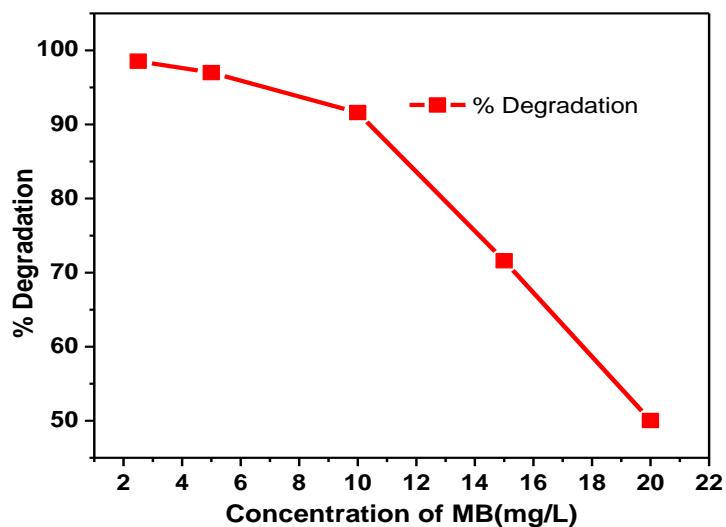


Figure 9. Effect of MB dye concentration on its photocatalytic degradation.

3.7.6. Effect of contact time.

The effect of contact time on the degradation efficiency of ZnO NPs (70 mg) on MB dye (30 mL of 10 mg L⁻¹) was studied at different contact times (0, 30, 60, 90, and 120 min) and at pH 10 (Figure 10). The experiment showed that degradation efficiency increased until the contact time reached 90 min, then remained constant. Therefore, the optimal exposure time for the enhanced degradation of 10 mg L⁻¹ MB dye using 70 mg ZnO was 90 min, yielding 94.7% degradation.

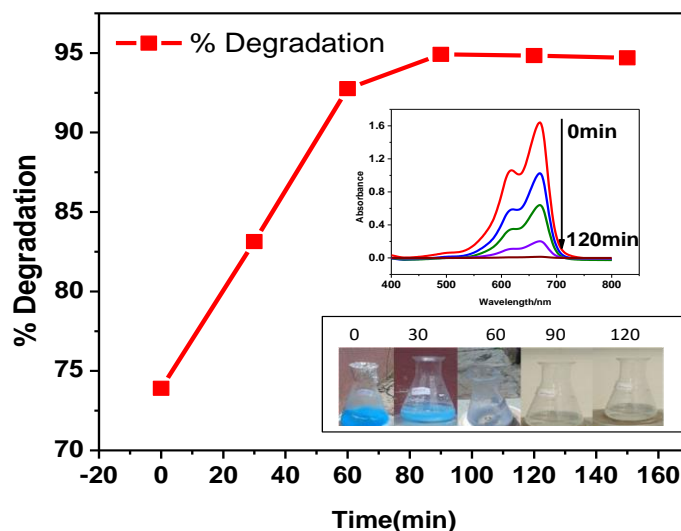


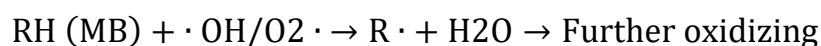
Figure 10. Effect of contact time on the degradation of MB dye by ZnO (70 mg) at pH 10, and the top inset shows the UV-vis spectrophotometer data of the MB degradation at different times.

The degradation efficiency of the catalyst, calculated from the absorbance of MB solutions after using the same ZnO NPs under similar test parameters in three photocatalytic degradation experiments, was 92.5%, 92.1%, and 91.3%, respectively. The complete disappearance of blue-like color to colorless provides conclusive proof of the catalyst's effectiveness (inset image, Figure 10). The top inset (Figure 10) shows the UV-Vis absorption

spectra (400-800 nm) of MB degradation at different contact/irradiation times. The average degradation efficiency of the catalyst (91.9%) demonstrated the photocatalytic recyclability of the synthesized ZnO NPs, with three cycles of oxidation of the MB dye.

3.8. Kinetic study of degradation of MB using ZnO NPs as a photocatalyst.

In this study, the synthesized ZnO NPs were used as a catalyst to degrade MB dye under direct sunlight. MB dye could not undergo degradation in direct sunlight radiation in the absence of a catalyst. Photocatalytic degradation of the dye over the surface of ZnO NPs was facilitated by the hydroxyl free radicals ($\cdot\text{OH}$) generated from water. The free radical initiates the oxidation of organic pollutant molecules (RH, MB) to CO_2 and H_2O through the removal of protons to produce highly reactive organic radicals ($\text{R}\cdot$) for further oxidation reactions. The schematic illustration of $\cdot\text{OH}$ generation for degradation of MB was reported elsewhere [3].



Since the water concentration is very high and did not change much during the photodegradation reaction, the reaction follows a pseudo-first-order kinetic model [46-48]. Thus, the rate equation expressed as equation 3 is rewritten as equation 4, as the rate of degradation is assumed to be independent of $[\cdot\text{OH}]$ [3,47,48], where the rate of disappearance of MB can be expressed using equations 5 and 6.

$$r = k[\text{MB}][\text{OH}\cdot] \quad (3)$$

$$r = k[\text{MB}] \quad (4)$$

$$r_{\text{MB}} = \frac{-\Delta[\text{MB}]}{\Delta t} = k[\text{MB}] \quad (5)$$

$$\frac{-d[\text{MB}]}{dt} = k[\text{MB}] \quad (6)$$

$$\ln[\text{MB}]_t = -kt + \ln[\text{MB}]_0 \quad (7)$$

Where: r_{MB} is the rate of disappearance of MB dye, $[\text{MB}]$ is the concentration of MB, k is the rate constant (min^{-1}), and t is the contact time (min).

It is observed that the rate of photocatalytic degradation of MB increases over time. The plot of $\ln C_0/C_t$ vs t (equation 7) results in a straight line whose slope ($k_1 = 0.05$, $R^2 = 0.996$) is characteristic of pseudo-first order kinetics (Figure 11).

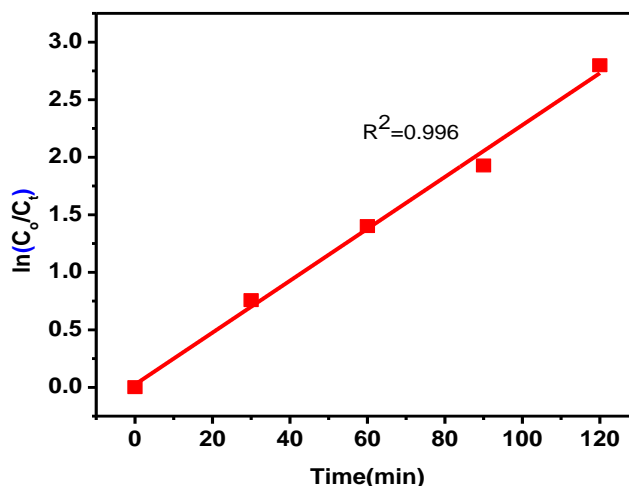


Figure 11. Graph of $\ln C_0/C_t$ of ZnO NPs vs time.

As the crystallite size of the ZnO NPs decreases, the nanostructure's available surface area increases; consequently, its catalytic activity increases. This study demonstrates a pseudo-first-order kinetic model for the photodegradation of MB-dyed contaminated water using nontoxic ZnO NPs synthesized from *A. esculentus* under sunlight irradiation. A promising degradation efficiency (94.7% for 10 mg L⁻¹ of MB dye) was observed for ZnO nanostructures as a photocatalyst at a dose of 70 mg, pH 10, and 90 min of irradiation.

4. Conclusion

A. esculentus seed aqueous extract supported the synthesis of highly crystalline ZnO NPs using Zn (CH₃CO₂)₂ · 2H₂O as precursor was effectively accomplished under an eco-friendly approach, and the NPs were characterized by XRD, SEM-EDS, FTIR, and UV-Vis techniques. The XRD pattern of ZnO shows a hexagonal wurzite structure with an average crystallite size of 14.5 nm. The SEM analysis showed that the average surface roughness and aggregated morphologies of ZnO NPs were 41.18, whereas the EDS spectra showed the presence of zinc (75%) and oxygen (15%). The higher photocatalytic efficiency (94.7 %) of the nanostructure was obtained under optimized working conditions, such as initial MB concentration (10 mg L⁻¹), pH (10), catalyst dose (70 mg), and contact time (90 min), which obeyed the pseudo-first-order kinetic model. The possible mechanism of the photocatalytic degradation of MB was its oxidation by •OH/O₂•⁻ generated in situ during the reaction. Therefore, the as-synthesized ZnO NPs were found to be an efficient and eco-friendly photocatalyst for the treatment of MB dye from aqueous solutions and/ or wastewater.

Author Contributions

Conceptualization, M.G. and A.N.; resources, M.G. and A.N.; methodology, M.G., A.N., N.B., and J.M.Y.; data interpretation, M.G. and A.N.; writing—original draft preparation, M.G. and A.N.; supervision, M.G. and A.N.; investigation, G.Y.; formal analysis, G.Y.; data curation, G.Y. and N.B.; software, N.B. and J.M.Y.; writing—review and editing, N.B. and J.M.Y.; validation, J.M.Y. All authors have read and agreed to the published version of this manuscript.

Institutional Review Board Statement

Not applicable.

Informed Consent Statement

Not applicable.

Data Availability Statement

Data supporting the findings of this study are available upon reasonable request from the corresponding author.

Funding

This research did not receive any specific grant from funding agencies.

Acknowledgments

We are grateful to Adama Science and Technology University (ASTU), Department of Materials Science and Engineering, for XRD analysis, and to Addis Ababa University, Department of Chemistry, for FTIR analysis. We also acknowledge Stellenbosch University, Institute for Nanotechnology and Water Sustainability, College of Science, Engineering and Technology, University of South Africa, Florida Science Campus, Johannesburg 1710, South Africa (Dr. Newaymedhin Abera) for SEM-EDS analysis.

Conflicts of Interest

The authors declare no conflict of interest.

References

1. Tang, J.; Zou, Z.; Yin, J.; Ye, J. Photocatalytic degradation of methylene blue on CaIn_2O_4 under visible light irradiation. *Chemical Physics Letters* **2003**, *382*, 175–179, <https://doi.org/10.1016/j.cplett.2003.10.062>.
2. Zheng, Y.; Qi, H.; Zhang, L.; Zhang, Y.; Zhong, L.; Zhang, X.; Feng, Y.; Xue, J. Photocatalytic degradation of dye wastewater by stepwise assembling PVA aerogel/ $\text{TiO}_2/\text{MoS}_2/\text{Au}$ composites in visible light. *Water Sci Technol* **2022**, *85*, 2625–2638, <https://doi.org/10.2166/wst.2022.106>.
3. Kahsay, M.H.; Tadesse, A.; RamaDevi, D.; Belachew, N.; Basavaiah, K. Green synthesis of zinc oxide nanostructures and investigation of their photocatalytic and bactericidal applications. *RSC Advances* **2019**, *9*, 36967–36981, <https://doi.org/10.1039/C9RA07630A>.
4. Adane, T.; Tiruneh, A.; Alemayehu, E. Textile Industry Effluent Treatment Techniques. *Journal of Chemistry* **2021**, *2021*, 1–14, <https://doi.org/10.1155/2021/5314404>.
5. Berradi, M.; Hsissou, R.; Khudhair, M.; Assouag, M.; Cherkaoui, O.; El Bachiri, A.; El Harfi, A. Textile finishing dyes and their impact on aquatic environs. *Heliyon* **2019**, *5*, 1–11, <https://doi.org/10.1016/j.heliyon.2019.e02711>.
6. Al-Tohamya, R.; Aliab, S.S.; Li, F.; Okasha, K.M.; G. Mahmoud, Y.A.; Elsamahy, T.; Jiao, H.; Fua, Y.; Sun, J. A Critical review on the treatment of dye-containing wastewater: Ecotoxicological and health concerns of textile dyes and possible remediation approaches for environmental safety. *Ecotoxicology and Environmental Safety* **2022**, *231*, 113160, <https://doi.org/10.1016/j.ecoenv.2021.113160>.
7. Valadez-Renteria, E.; Oliva, J.; Rodriguez-Gonzalez, V. Photocatalytic materials immobilized on recycled supports and their role in the degradation of water contaminants: A timely review. *Science of The Total Environment* **2022**, *807*, 1500820, <https://doi.org/10.1016/j.scitotenv.2021.150820>.
8. Khan, I.; Saeed, K.; Zekker, I.; Zhang, B.; Hendi, A.H.; Ahmad, A.; Ahmad, S.; Zada, N.; Ahmad, H.; Shah, L.A.; Shah, T. Review on Methylene Blue: Its Properties, Uses, Toxicity and Photodegradation. *Water* **2022**, *14*, 242, <https://doi.org/10.3390/w14020242>.
9. Patel, R.K.; Prasad, R.; Shankar, R.; Khare, P.; Yadav, M. Adsorptive Removal of Methylene Blue Dye from Soapnut Shell & Pineapple Waste Derived Activated Carbon. *International Journal of Engineering, Science and Technology* **2021**, *13*, 81–87, <https://doi.org/10.4314/ijest.v13i1.12s>.
10. Belachew, N.; Hinsene, H. Preparation of Zeolite 4A for Adsorptive removal of Methylene Blue: optimization, Kinetics, Isotherm and mechanism Study. *Silicon* **2022**, *14*, 1629–1641, <https://doi.org/10.1007/s12633-020-00938-9>.
11. Karaer, H.; Kaya, I. Synthesis, characterization of magnetic chitosan/active charcoal composite and using at the adsorption of methylene blue and reactive blue. *Microporous and Mesoporous Material* **2016**, *232*, 26–38, <https://doi.org/10.1016/j.micromeso.2016.06.006>.
12. Hassan, M. A.; El-Nemr, A. Health and environmental impacts of dyes, minireview. *AJESE* **2017**, *1*, 64–67.
13. Kavitha, G.; Kumar, J.V.; Devanesan, S.; Asemi, N.N.; Manikandan, V.; Arulmozhi, R.; Abirami, N. Ceria nanoparticles anchored on graphitic oxide sheets ($\text{CeO}_2\text{-GOS}$) as an efficient catalyst for degradation of dyes and textile effluents. *Environmental Research* **2022**, *209*, 112750, <https://doi.org/10.1016/j.envres.2022.112750>.
14. Licayan, K.D.O.; Manigo, J.P.; Oracion, J.P.L.; De La Rosa, L.B.; Alguno, A.C.; Deocarlis, C.C.; Capangpangan, R.Y. Synthesis and characterization of $\text{Fe}_3\text{O}_4/\text{BiOCl}/\text{Cu}_2\text{O}$ composite as photocatalyst for the degradation of organic dyes. *Materials Today: Proceedings* **2021**, *46*, 1663–1667, <https://doi.org/10.1016/j.matpr.2020.07.262>.
15. Belachew, N.; Hagos, M.; Tadesse, A.; Basavaiah, K. Green synthesis of reduced graphene oxide grafted Ag/ZnO for photocatalytic abatement of methylene blue and antibacterial activities. *Journal of Environmental Chemical Engineering* **2020**, *8*, 104106, <https://doi.org/10.1016/j.jece.2020.104106>.

16. Kiwaan, H.A.; Atwee, T.M.; Azab, E.A.; El-Bindary, A.A. Photocatalytic degradation of organic dyes in the presence of nanostructured titanium dioxide. *Journal of Molecular Structure* **2020**, *1200*, 12715, <https://doi.org/10.1016/j.molstruc.2019.127115>.
17. Priyadarshini, S.S.; Shubha, J.P.; Shivalingappa, J.; Adil, S.F.; Kuniyil, M.; Hatshan, M.R.; Shaik, B.; Kavalli, K. Photocatalytic Degradation of Methylene Blue and Metanil Yellow Dyes Using Green Synthesized Zinc Oxide (ZnO) Nanocrystals. *Crystals* **2022**, *12*, 22, <https://doi.org/10.3390/cryst12010022>.
18. Arumugasamy, S.K.; Ramakrishnan, S.; Yoo, J.D.; Govindaraju, S.; Yun, K. Tuning the interfacial electronic transitions of bi-dimensional nanocomposites (pGO/ZnO) towards photocatalytic degradation and energy application. *Environmental Research* **2022**, *204*, 112050, <https://doi.org/10.1016/j.envres.2021.112050>.
19. Vikraman, D.; Patil, S.S.; Hussain, S.; Hussain, M.; Karuppasamy, K.; Santhoshkumar, P.; Lee, J.H.; Lee, K.; Jung, J.; Kim, H.S. Decoration of X2C nanoparticles on CdS nanostructures for highly efficient photocatalytic wastewater treatment under visible light. *Applied Surface Science* **2022**, *583*, 152533, <https://doi.org/10.1016/j.apsusc.2022.152533>.
20. Jiang, D.; Otitoju, T.A.; Ouyang, Y.; Shoparwe, N.F.; Wang, S.; Zhang, A.; Li, S. A Review on Metal Ions Modified TiO₂ for Photocatalytic Degradation of Organic Pollutants. *Catalysts* **2021**, *11*, 1039, <https://doi.org/10.3390/catal11091039>.
21. Nazim, M.; Aslam, A.; Khan, P.; Asiri, A.M.; Kim, J.H. Exploring Rapid Photocatalytic Degradation of Organic Pollutants with Porous CuO Nanosheets: Synthesis, Dye Removal, and Kinetic Studies at Room Temperature. *ACS Omega* **2021**, *6*, 2601–2612, <https://doi.org/10.1021/acsomega.0c04747>.
22. Tadesse, A.; Hagos, M.; Belachew, N.; Ananda Murthy, H.C.; Basavaiah, K. Enhanced photocatalytic degradation of Rhodamine B, antibacterial and antioxidant activities of green synthesised ZnO/N doped carbon quantum dot nanocomposites. *New Journal of Chemistry* **2021**, *45*, 21852-21862, <https://doi.org/10.1039/D1NJ04036G>.
23. Belachew, N.; Fekadu, R.; Abebe, A.A. RSM-BBD Optimization of Fenton-Like Degradation of 4-Nitrophenol Using Magnetite Impregnated Kaolin. *Air, Soil and Water Research* **2020**, *13*, 1-10, <https://doi.org/10.1177/1178622120932124>.
24. El Shafey, A.M. Green synthesis of metal and metal oxide nanoparticles from plant leaf extracts and their applications: A review. *Green Processing and Synthesis* **2020**, *9*, 304-339, <https://doi.org/10.1515/gps-2020-0031>.
25. Isai, K.A.; Shrivastava, V.S. Photocatalytic degradation of methylene blue using ZnO and 2%Fe–ZnO semiconductor nanomaterials synthesized by sol–gel method: a comparative study. *SN Applied Science* **2019**, *1*, <https://doi.org/10.1007/s42452-019-1279-5>.
26. Habtamu, F.G.; Haki, G.D.; Fekadu, B.; Rakshit, S.K.; Ashagrie, Z.W. Nutritional and antinutritional evaluation of indigenous Ethiopian okra (*Abelmoschus esculentus*) seed accessions. *African Journal of Food, Agriculture, Nutrition and Development* **2018**, *18*, 13019-13033, <https://doi.org/10.18697/ajfand.81.16515>.
27. Islam, M.T.; Phytochemical information and pharmacological activities of Okra (*Abelmoschus esculentus*): A literature-based review. *Phytotherapy research* **2019**, *33*, 72-80, <https://doi.org/10.1002/ptr.6212>.
28. Adelakun, O.E.; Oyelade, O.J.; Ade-Omowaye, B.I.; Adeyemi, I.A.; Van de Venter, M. Chemical composition and the antioxidative properties of Nigerian okra seed (*Abelmoschus esculentus* Moench) flour. *Food and Chemical Toxicology* **2009**, *47*, 1123–6, <https://doi.org/10.1016/j.fct.2009.01.036>.
29. Liao, H.; Liu, H.; Yuan, K. A new flavonol glycoside from the *Abelmoschus esculentus* Linn. *Pharmacognosy Magazine* **2012**, *8*, 12–5, <https://doi.org/10.4103/0973-1296.93303>.
30. Arapitsas, P. Identification and quantification of polyphenolic compounds from okraseeds and skins. *Food Chemistry* **2008**, *110*, 1041–1045, <https://doi.org/10.1016/j.foodchem.2008.03.014>.
31. Romdhane, M. H.; Chahdoura, H.; Barros, L.; Dias, M. I.; Corrêa, R. C. G.; Morales, P.; Ferreira, I. C. Chemical composition, nutritional value, and biological evaluation of Tunisian okra pods (*Abelmoschus esculentus* L. Moench). *Molecules* **2020**, *25*, 4739, <https://doi.org/10.3390/molecules25204739>.
32. Liu, I.M.; Tzeng, T.F.; Liou, S.S. *Abelmoschus moschatus* (Malvaceae), an aromatic plant, suitable for medical or food uses to improve insulin sensitivity. *Phytotherapy Research* **2010**, *24*, 233–239, <https://doi.org/10.1002/ptr.2918>.
33. Dantas, T.L.; Alonso Buriti, F.C.; Florentino, E.R. Okra (*Abelmoschus esculentus* L.) as a Potential Functional Food Source of Mucilage and Bioactive Compounds with Technological Applications and Health Benefits. *Plants* **2021**, *10*, 1683, <https://doi.org/10.3390/plants10081683>.
34. Sabitha, V.; Ramachandran, S.; Naveen, K.R.; Panneerselvam, K. Antidiabetic and antihyperlipidemic potential of *Abelmoschus esculentus* (L.) Moench. in streptozotocin-induced diabetic rats. *Journal of Pharmacy and Bioallied Science* **2011**, *3*, 397–402, <https://doi.org/10.4103/0975-7406.84447>.
35. Faisal, S.; Jan, H.; Shah, S. A.; Shah, S.; Khan, A.; Taj Akbar M.; Rizwan, M.; Jan, F.; Akhtar, N.; Khattak, A.; Syed, S. Green Synthesis of Zinc Oxide (ZnO) Nanoparticles Using Aqueous Fruit Extracts of *Myristica fragrans*: Their Characterizations and Biological and Environmental Applications *ACS Omega* **2021**, *6*, 9709–9722, <https://doi.org/10.1021/acsomega.1c00310>.

36. Asker, M.; El-gengaihi, S.E.; Hassan, E.M.; Mohammed, M.A.; Abdelhamid, S.A. Phytochemical Constituents and Antibacterial Activity of Citrus Lemon Leaves. *Bulletin of the National Research Centre* **2020**, *44*, 1–7, <https://doi.org/10.1186/s42269-020-00446-1>.
37. Mourdikoudis, S.; Pallares, R.M.; Thanh, N.T.K. Characterization Techniques for Nanoparticles: Comparison and Complementarity upon Studying Nanoparticle Properties. *Nanoscale* **2018**, *10*, 12871–12934, <https://doi.org/10.1039/c8nr02278j>.
38. Jenkins, R.; Snyder, R.L. Introduction to X-Ray Powder Diffraction. John Wiley & Sons: **1996**; <https://doi.org/10.1002/9781118520994>.
39. Tefera, M.; Fekadu, R.; Eshete, F. F.; Kabtamu, D. M.; Gashu, M.; Tadesse, A.; Belachew, N. Visible-light-driven reduction of chromium (VI) by green synthesised cuprous oxide nanoparticles. *Journal of Molecular Liquids* **2022**, *359*, 119272, <https://doi.org/10.1016/j.molliq.2022.119272>.
40. Shaba, E.Y.; Jacob, J.O.; Tijani, J.O.; Suleiman, M.A.T. A Critical Review of Synthesis Parameters Affecting the Properties of Zinc Oxide Nanoparticle and Its Application in Wastewater Treatment. *Applied Water Science* **2021**, *11*, 1-48, <https://doi.org/10.1007/s13201-021-01370-z>.
41. Mahmood, T.; Saddique, M. T.; Naeem, A.; Westerhoff, P.; Mustafa, S.; Alum, A. Comparison of Different Methods for the Point of Zero Charge Determination of NiO. *Industrial & Engineering Chemistry Research* **2011**, *50*, 10017–10023, <https://doi.org/10.1021/ie200271d>.
42. Klinton, D.; Yarbrough, R.; Froeschle, M.; White, J.; Rathnayake, H. Band gap engineered zinc oxide nanostructures via a sol–gel synthesis of solvent driven shape-controlled crystal growth. *RSC advances* **2019**, *9*, 14638-14648, <https://doi.org/10.1039/C9RA02091H>.
43. Ahmed, Z. O.; Aragaw, S. G.; Sabir, F. K.; Andoshe, D. M.; Duma, A. D.; Kuo, D-H.; Chen, X. et al. Green synthesis of Co-doped ZnO via the accumulation of cobalt ion onto Eichhornia crassipes plant tissue and the photocatalytic degradation efficiency under visible light. *Materials Research Express* **2021**, *8*, 025010, <https://doi.org/10.1088/2053-1591/abe2d6>.
44. Cho, E.J.; Holback, H.; Liu, K. C.; Abouelmagd, S. A.; Park, J.; Yeo, Y. Nanoparticle Characterization: State of the Art, Challenges, and Emerging Technologies. *Molecular Pharmaceutics* **2013**, *10*, 2093–2110, <https://doi.org/10.1021/mp300697h>.
45. Sposito, G.J. Soil Science Society of America Journal. *The operational definition of the zero point of charge in soils* **1981**, *45*, 292-297, <https://doi.org/10.2136/sssaj1981.03615995004500020013x>.
46. Fosso-Kankeu, E.; Pandey, S.; Ray, S.S. Photocatalysts in Advanced Oxidation Processes for Wastewater Treatment. John Wiley & Sons: **2020**; <https://doi.org/10.1002/9781119631422>.
47. Hung, N.V.; Nguyet, B.T.M.; Huu Nghi, N.; Khieu, D.Q. Photocatalytic Degradation of Methylene Blue by using ZnO/ Longan Seed Activated Carbon under Visible-Light Region. *Journal of Inorganic and Organometallic Polymers and Materials* **2020**, *31*, 446-459, <https://doi.org/10.1007/s10904-020-01734-z>.
48. Singh, J.; Chang, Y.-Y.; Koduru, J.R.; Yang, J.-K. Potential Degradation of Methylene Blue (MB) by NanoMetallic Particles: A Kinetic Study and Possible Mechanism of MB Degradation. *Environmental Engineering Research* **2018**, *23*, 1–9, <https://doi.org/10.4491/eer.2016.158>.

Publisher’s Note & Disclaimer

The statements, opinions, and data presented in this publication are solely those of the individual author(s) and contributor(s) and do not necessarily reflect the views of the publisher and/or the editor(s). The publisher and/or the editor(s) disclaim any responsibility for the accuracy, completeness, or reliability of the content. Neither the publisher nor the editor(s) assume any legal liability for any errors, omissions, or consequences arising from the use of the information presented in this publication. Furthermore, the publisher and/or the editor(s) disclaim any liability for any injury, damage, or loss to persons or property that may result from the use of any ideas, methods, instructions, or products mentioned in the content. Readers are encouraged to independently verify any information before relying on it, and the publisher assumes no responsibility for any consequences arising from the use of materials contained in this publication.